Defence Research and Development Canada
Recherche et développement pour la défense Canada

DEFENCE R&D DÉFENSE

Micro-Doppler signal estimation for rotating targets from a fraction of the period

T. Thayaparan, L. Stankovic, M. Dakovic and V. Popovic

Defence R&D Canada – Ottawa

Canada

Technical Memorandum
DRDC Ottawa TM 2009-280
February 2010

Micro-Doppler signal estimation for rotating targets from a fraction of the period

T. Thayaparan
Defence R&D Canada – Ottawa

L. Stankovic, M. Dakovic, V. Popovic
University of Montenegro

Defence R&D Canada – Ottawa
Technical Memorandum
DRDC Ottawa TM 2009-280
February 2010

Principal Author

Original signed by T. Thayaparan

T. Thayaparan

Approved by

Original signed by Caroline Wilcox

Caroline Wilcox
Defence Scientist/RAST Section

Approved for release by

Original signed by Brian Eatock

Brian Eatock
Chair/Document Review Panel

Abstract

Radar micro-Doppler signatures are of great potential for identifying properties of unknown targets. All the techniques developed for extracting micro-Doppler features for the past decade rely primarily on the assumption that the time series of the signal contains at least one oscillation or more during the coherent integration time or imaging time. However, many applications in real-world scenarios involve short duration signals and often require the detection and the estimation of micro-Doppler characteristics. Short duration signals may contain only a fraction of an oscillation. In this report, we develop two techniques to estimate the micro-Doppler parameters from a fraction of the period. In these scenarios, the coherent integration will cover only 1/4 and 1/2 of the oscillation. The performance of the proposed methods are evaluated using both synthetic and experimental data.

Résumé

Les signatures radar obtenues par microdécalage Doppler présentent un grand potentiel pour la reconnaissance des propriétés des cibles inconnues. Toutes les techniques mises au point pour extraire les caractéristiques de microdécalage Doppler au cours de la dernière décennie reposent principalement sur la présomption que la suite temporelle d'un signal contient au moins une oscillation au cours de l'intervalle d'intégration cohérente ou de l'intervalle d'imagerie. Toutefois, bon nombre d'applications dans des scénarios réels utilisent des signaux de courte durée et nécessitent souvent la détection et l'estimation des caractéristiques de microdécalage Doppler. Les signaux de courte durée peuvent contenir seulement une fraction d'une oscillation. Dans le présent rapport, nous élaborons deux techniques pour estimer les paramètres du microdécalage Doppler à partir d'une fraction de la période. Dans ces scénarios, l'intégration cohérente vise seulement le quart et la moitié de l'oscillation. Les performances des méthodes proposées font l'objet d'une évaluation à partir de données synthétiques et expérimentales.

This page intentionally left blank.

Executive summary

Micro-Doppler signal estimation for rotating targets from a fraction of the period

T. Thayaparan, L. Stankovic, M. Dakovic, V. Popovic; DRDC Ottawa TM 2009-280; Defence R&D Canada – Ottawa; February 2010.

Background: Today radar technology has attained a broad scope of applications ranging from military to civilian. Target classification is one such area, which investigates both the moving characteristics as well as discrimination of targets. Recent research indicates that the micro-Doppler technique exhibits a high potential for this purpose. The basic idea behind this is that mechanical vibration or rotation of a target, or structures on the target, may induce additional frequency modulations to the regular Doppler shift on the returned radar signal. This generates sidebands about the target's Doppler frequency, called micro-Doppler effect. Micro-Doppler is regarded as unique signature and can be used to determine properties of a target. The uniqueness of micro-Doppler signatures means different micro-motions have distinct signatures. All the techniques developed for the past decade for extracting micro-Doppler features rely primarily on the assumption that the time series of the signal contains at least one oscillation or more during the coherent integration time or imaging time. However, many applications in realistic real-world scenarios involve short duration signals such as rotating antenna on a ship or ground, rotating blades of the aircraft/helicopter, etc. These applications often require detection and estimation of micro-Doppler characteristics. Short duration signals may contain only a fraction of an oscillation. In this report, we develop two techniques to estimate the micro-Doppler parameters from a fraction of the period. In these scenarios, the coherent integration will cover only a fraction of the oscillation.

Results: We have developed two techniques to estimate the micro-Doppler parameters from a fraction of the period. In these scenarios, the coherent integration covers only 1/4 and 1/2 of the oscillation. The first method is based on a three-point model and the second method is based on a cubic polynomial fitting and a approximation. The reliability and robustness of these two methods are evaluated using both simulated and experimental data. Both proposed methods have shown satisfactory accuracy for both simulated and experimental data.

Significance: Micro-Doppler features have great potential for use in automatic target classification algorithms. Although there have been studies of m-D effects in radar in the past few years, this is the first study for micro-Doppler parameter estimation from a fraction of the period, that has great potential for use in target identification applications. As such, this report contributes additional experimental m-D data and

analysis, which should help in developing a better picture of the m-D research and its applications to indoor and outdoor radar detection and automatic gait recognition systems. The two techniques developed in this study can also be used to evaluate the motion parameters of the rotating antenna on a ship or ground using RADARSAT data. Alternatively, these techniques can also be used to extract biometric information related to periodic contraction of a heart, blood vessels, lungs, other fluctuations of the skin in the process of breathing and heart beating, which should help in human m-D research and its applications to through-wall radar imaging.

Sommaire

Micro-Doppler signal estimation for rotating targets from a fraction of the period

T. Thayaparan, L. Stankovic, M. Dakovic, V. Popovic ; DRDC Ottawa
TM 2009-280 ; R & D pour la défense Canada – Ottawa ; février 2010.

Contexte : La technologie radar d'aujourd'hui donne lieu à une grande diversité d'applications militaires et civiles. La classification des cibles est l'une de ces applications. Elle porte sur l'examen des caractéristiques de déplacement et la discrimination des cibles. De récentes recherches soutiennent que la technique du microdécalage Doppler présente un énorme potentiel en ce sens. Le concept sous-jacent est que les vibrations mécaniques ou la rotation d'une cible ou de ses structures peuvent induire d'autres modulations de fréquence, outre le décalage Doppler normal du signal radar capté. Il en résulte des bandes latérales autour de la fréquence Doppler de la cible, ce que nous appelons l'effet du microdécalage Doppler. Cet effet constitue une signature distincte et peut servir à déterminer les propriétés d'une cible. L'unicité des signatures du microdécalage Doppler signifie que les divers micromouvements ont des signatures distinctes. Toutes les techniques élaborées au cours de la dernière décennie pour extraire les caractéristiques du microdécalage Doppler reposent principalement sur la présomption que la suite temporelle du signal contient au moins une oscillation durant l'intervalle d'intégration cohérente ou l'intervalle d'imagerie. Toutefois, bon nombre d'applications du monde réel font appel à des signaux de courte durée, comme la rotation d'une antenne sur un navire ou au sol, les pales tournantes d'un avion ou d'un hélicoptère, etc. Ces applications nécessitent souvent la détection et l'estimation des caractéristiques du microdécalage Doppler. Les signaux de courte durée peuvent contenir seulement une fraction d'une oscillation. Dans le présent rapport, nous élaborons deux techniques pour estimer les paramètres du microdécalage Doppler à partir d'une fraction de la période. Dans ces scénarios, l'intégration cohérente vise seulement une fraction de l'oscillation.

Résultats : Nous avons élaboré deux techniques pour estimer les paramètres du microdécalage Doppler à partir d'une fraction de la période. Dans ces scénarios, l'intégration cohérente vise seulement le quart et la moitié de l'oscillation. La première méthode repose sur un modèle à trois points, et la seconde méthode recourt à une fonction polynomiale cubique et à une approximation. La fiabilité et la robustesse de ces deux méthodes sont évaluées au moyen de données simulées et de données expérimentales. Les deux méthodes proposées ont démontré une précision satisfaisante à partir des deux types de données.

Portée : Les caractéristiques du microdécalage Doppler ont un grand potentiel dans

les algorithmes de classification automatique des cibles. Bien qu'il y ait eu des études sur les effets du microdécalage Doppler dans le domaine du radar au cours des dernières années, la présente étude est la première portant sur l'estimation des paramètres du microdécalage Doppler à partir d'une fraction de la période. Et la technique présente un grand potentiel dans les applications d'identification des cibles. En ce sens, le présent rapport fait part de nouvelles données expérimentales et d'une analyse du microdécalage Doppler qui devrait aider à l'obtention d'un meilleur tableau de la recherche sur le microdécalage Doppler et de ses applications dans les systèmes radar de détection et les systèmes automatiques de reconnaissance du mouvement, intérieurs et extérieurs. Les deux techniques abordées dans la présente étude pourront aussi servir à évaluer les paramètres de déplacement de l'antenne rotative installée sur un navire ou au sol à partir des données de RADARSAT. D'un autre côté, ces techniques pourront aussi servir à extraire les renseignements biométriques propres à la contraction périodique du cœur, des vaisseaux sanguins et des poumons et aux mouvements de la peau durant la respiration et les battements du cœur. Toutes ces données devraient aider à la recherche sur le microdécalage Doppler à l'égard de l'humain et à ses applications dans le domaine de l'imagerie radar passe-muraille.

Table of contents

List of figures

Acknowledgements

We would like to thanks Prof. Moeness Amin, Villanova University for supplying to us the indoor rotating fan data. We would like to thank E. Riseborough, D. Lamothe, and G. Duff for their support during experimental trials and data collection.

1 Introduction

Today's radar technology has attained a broad scope of applications ranging from military to civilian. Target classification is one such area, which investigates both the moving characteristics as well as discrimination of targets. Recent research indicates that the micro-Doppler (m-D) technique exhibits a high potential for this purpose. The basic idea behind this is that mechanical vibration or rotation of a target, or structures on the target, may induce additional frequency modulations to the regular Doppler shift on the returned radar signal. This generates sidebands about the target's Doppler frequency, called micro-Doppler effect. Micro-Doppler is regarded as a unique signature and can be used to determine properties of a target. The uniqueness of micro-Doppler signatures means different micro-motions have distinct signatures [1]-[10].

Traditional techniques, such as Fourier analysis or the sliding window Fourier transform (FT) (short time Fourier transform - STFT), lack the required resolution for extracting and processing these unique m-D features. Therefore, high-resolution linear and quadratic time-frequency (TF) analysis techniques are recently employed for extracting m-D features [1]-[3],[5]-[6],[7],[9]. Several reports have been written about the ways to deal with the m-D effect. Wavelet analysis of helicopter and human data, along with the TF representation based imaging system, is presented in reference [2]. Details on the m-D effect physics, with some typical examples, are given in reference [5]. A method for the separation of the m-D effect from the radar image, based on the chirplet transform, is proposed in [7]. Both wavelet-based and chirplet-based procedures are used in reference [8] to extract m-D features such as the rotating frequency of an antenna in SAR (synthetic aperture radar) data. Recently, two techniques for the separation of a target's rigid body from m-D parts have been proposed in reference [9]. The first approach is based on order statistics of the spectrogram samples. The second approach is based on the Radon transform processing of obtained radar signals. An effective quadratic time-frequency S-method based approach in conjunction with the Viterbi algorithm to extract m-D features is proposed in [3].

All the techniques developed for the past decade rely primarily on the assumption that the time series of the signal contains at least one oscillation or more during the coherent integration time or imaging time. However, many applications in realistic real-world scenarios involve short duration signals and often require detection and estimation of micro-Doppler characteristics. Short duration signals may contain only a fraction of an oscillation. In this report, we develop two techniques to estimate the micro-Doppler parameters from a fraction of the period. In these scenarios, the coherent integration will cover only $\frac{1}{4}$ and $\frac{1}{2}$ of the oscillation.

The report is organized as follows. Two estimation methods are presented in Section 2. The demonstration of the proposed methods using the simulated data is presented

in Section 3. The application to the real radar data is given in Section 4. In Section 5, conclusions are given.

2 Estimation methods

It is known that mechanical vibration or rotation on a target can induce frequency modulation on the returned radar signal and generates sidebands about the Doppler frequency shift of the target's body [4, 5]. The frequency of the returned radar signal is time dependent and can be modeled as (see Figure 1)

$$f(t) = f_0 + A\cos(2\pi f_v t + \theta), \tag{1}$$

where f_0 is the Doppler frequency caused by the target motion and $A\cos(2\pi f_v t + \theta)$ is the Doppler frequency caused by vibrating or rotating parts. Here f_v denotes the frequency of the rotation (or vibration), and θ is an arbitrary phase angle. Thus, the radar return can be written as

$$x(t) = \exp(j2\pi f_0 + j\frac{A}{f_v}\sin(2\pi f_v t + \theta)). \tag{2}$$

We will assume that the instantaneous frequency of the radar return is estimated by using the time-frequency analysis methods as described in [13, 14] giving the estimation

$$\hat{f}(t) \approx f_0 + A\cos(2\pi f_v t + \theta) \tag{3}$$

Our goal is to estimate the target rotation (or vibration) rate f_v. We will assume that the observation interval $0 \leq t < T$ is small, i.e., $2\pi f_v T < \pi$. In this case, we can not perform the conventional estimation methods for f_v (e.g., Fourier-based, zero crossing based methods, etc.). In this section, we develop two approaches to estimate the micro-Doppler parameters from a fraction of the period.

2.1 Estimation Method-1

In the first approach, we use a 3-point model to estimate the motion parameters from a fraction of the period. Figure 1 shows the illustration of the method for frequency determination based on a 3-point model. Let us consider the discrete sinusoidal signal

$$y(n) = A\sin(\omega n + \varphi), \tag{4}$$

where A is the amplitude, ω is the angular discrete frequency, and initial phase φ is the initial phase.

The frequency of the considered signal can be estimated as

$$\omega_e = \frac{1}{k}\arccos\frac{y(n-k) + y(n+k)}{2y(n)}. \tag{5}$$

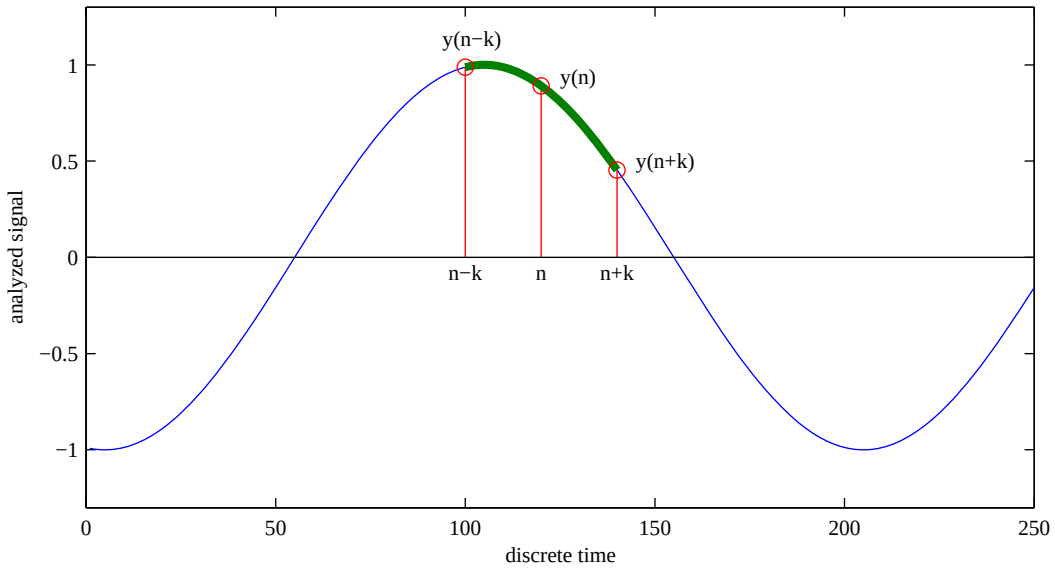

Figure 1: *Illustration of the method for frequency determination based on three points for* $n = 120$ *and* $k = 20$

Proof:

$$\frac{y(n-k)+y(n+k)}{2y(n)} = \frac{A\sin(\omega n+\varphi-\omega k)+A\sin(\omega n+\varphi+\omega k)}{2A\sin(\omega n+\varphi)} = \\ = \frac{2A\sin(\omega n+\varphi)\cos(\omega k)}{2A\sin(\omega n+\varphi)} = \cos(\omega k) \tag{6}$$

$$\omega_e = \frac{1}{k}\arccos(\cos(\omega k)) = \omega = \frac{1}{k}\arccos\left(\frac{y(n-k)+y(n+k)}{2y(n)}\right) \tag{7}$$

Note that ω should be $0 \leq \omega \leq \pi/k$. This relation limits the values of lag k to several samples, which is not so important since ω is assumed to be small in this case. In this scenario, the considered time interval is much smaller than half of the period.

In the case of noisy observations

$$\hat{y}(n) = y(n) + \varepsilon(n), \tag{8}$$

where $\varepsilon(n)$ is a discrete noise. When an estimation error is introduced, Equation 5 becomes:

$$\cos(\omega k) = \frac{y(n-k)+\varepsilon(n-k)+y(n+k)+\varepsilon(n+k)}{2y(n)+2\varepsilon(n)}. \tag{9}$$

For small $\varepsilon(n)$ compared to $y(n)$ and by using the well-known approximation $(1/(1+x) \approx 1-x$ for small $x)$ we get

$$\frac{1}{2y(n)+2\varepsilon(n)} = \frac{1}{2y(n)} \frac{1}{1+\frac{\varepsilon(n)}{y(n)}} \approx \frac{1}{2y(n)}(1-\frac{\varepsilon(n)}{y(n)}). \tag{10}$$

Thus, we can write

$$\cos(\omega k) = (y(n-k)+\varepsilon(n-k)+y(n+k)+\varepsilon(n+k)) \frac{1}{2y(n)}(1-\frac{\varepsilon(n)}{y(n)}). \tag{11}$$

By neglecting the higher-order error terms such as $(\varepsilon(n)\varepsilon(n+k)$ and $\varepsilon(n)\varepsilon(n-k)$, small error multiplied by small error), the error ξ in the estimation of $\cos(\omega k)$ is:

$$\begin{aligned}
\xi &= \cos(\omega k)|_{with_noise} - \cos(\omega k)|_{without_noise} \\
&= \frac{y(n-k)+\varepsilon(n-k)+y(n+k)+\varepsilon(n+k)}{2y(n)}(1-\frac{\varepsilon(n)}{y(n)}) - \\
&\quad -\frac{y(n-k)+y(n+k)}{2y(n)} \\
&= \left(\frac{y(n-k)+y(n+k)}{2y(n)} + \frac{\varepsilon(n-k)+\varepsilon(n+k)}{2y(n)}\right)(1-\frac{\varepsilon(n)}{y(n)}) - \\
&\quad -\frac{y(n-k)+y(n+k)}{2y(n)} \\
&\approx \frac{\varepsilon(n-k)+\varepsilon(n+k)}{2y(n)} - \frac{y(n-k)+y(n+k)}{2y(n)}\frac{\varepsilon(n)}{y(n)}
\end{aligned} \tag{12}$$

$$\xi = \frac{\varepsilon(n-k)+\varepsilon(n+k)}{2y(n)} - \cos(\omega k)\frac{\varepsilon(n)}{y(n)} \tag{13}$$

The mean of the estimation error is equal to zero. This means that the estimator is unbiased. The variance of ξ is equal to the mean square of the estimation error

$$var(\xi) = E[\xi^2], \tag{14}$$

where $E[\cdot]$ is the expectation operator. If we assume that $\varepsilon(n-k)$, $\varepsilon(n+k)$ and $\varepsilon(k)$ are mutually independent, the sum of three independent random variables is

$$\xi = \frac{\varepsilon(n-k)}{2y(n)} + \frac{\varepsilon(n+k)}{2y(n)} - \cos(\omega k)\frac{\varepsilon(n)}{y(n)}, \tag{15}$$

and the total variance is equal to the sum of individual variances

$$var(\xi) = var(\frac{\varepsilon(n-k)}{2y(n)}) + var(\frac{\varepsilon(n+k)}{2y(n)}) + var(-\cos(\omega k)\frac{\varepsilon(n)}{y(n)}), \tag{16}$$

with

$$var(\frac{\varepsilon(n-k)}{2y(n)}) = \frac{1}{4y(n)^2}var(\varepsilon(n-k)) = \frac{\sigma_e^2}{4y(n)^2}, \quad (17)$$

$$var(\frac{\varepsilon(n+k)}{2y(n)}) = \frac{1}{4y(n)^2}var(\varepsilon(n+k)) = \frac{\sigma_e^2}{4y(n)^2}, \quad (18)$$

$$var(-\cos(\omega k)\frac{\varepsilon(n)}{y(n)}) = \frac{\cos^2(\omega k)}{y(n)^2}var(\varepsilon(n)) = \frac{\cos^2(\omega k)}{y(n)^2}\sigma_e^2. \quad (19)$$

Finally the variance of ξ is:

$$\begin{aligned} var(\xi) &= \frac{\sigma_e^2}{4y(n)^2} + \frac{\sigma_e^2}{4y(n)^2} + \frac{\cos^2(\omega k)}{y(n)^2}\sigma_e^2 \\ &= \frac{\sigma_\varepsilon^2}{2y(n)^2}(1 + 2\cos^2(\omega k)) \\ &= \frac{(2+\cos(2\omega k))}{2}\frac{\sigma_\varepsilon^2}{y(n)^2} \\ &= \frac{(2+\cos(2\omega k))}{2}\frac{1}{SNR_n}. \end{aligned} \quad (20)$$

where SNR_n is signal-to-noise ratio at the time instant n and we assume that noise samples $\varepsilon(n-k)$, $\varepsilon(n)$ and $\varepsilon(n+k)$ are independent with variance σ_ε^2. For small ωk, $\cos(2\omega k) \approx 1$ and we finally get

$$var(\xi) \approx \frac{3}{2}\frac{1}{SNR}. \quad (21)$$

The most significant component of the noise is related to the discretization error in the estimation of the instantaneous frequency using the discrete frequency grid. The simplest way to reduce this error is by using several points, n, and several lags, k, to obtain set of estimates

$$\Omega = \{\omega_{e,n,k}\}, \quad (22)$$

and the resulting estimate, that is, the mean value of such estimates is,

$$\hat{\omega}_e = \underset{\omega_{e,n,k}\in\Omega}{mean}\ \omega_{e,n,k}. \quad (23)$$

Assuming that estimations $\omega_{e,n,k}$ are statistically independent, the variance of the resulting estimation error is

$$var(\xi_e) = \frac{var(\xi_{e,n,k})}{N_\Omega}, \quad (24)$$

where N_Ω is number of independent estimations, i.e. the number of elements of the set Ω.

2.2 Estimation Method-2

In the second approach, we use cubic polynomial fitting to estimate the motion parameters from a fraction of the period. Let us consider the signal of the form

$$y(n) = A\sin(\omega n + \varphi) + B, \tag{25}$$

with $\omega \ll 1$. The signal can be expanded into Taylor series around $n = 0$ as

$$\begin{aligned} y(n) &= y(0) + \frac{y'(0)}{1!}n + \frac{y''(0)}{2!}n^2 + \frac{y'''(0)}{3!}n^3 + \cdots = & (26)\\ &= A\sin(\varphi) + B + A\omega\cos(\varphi)n - \frac{A\omega^2\sin(\varphi)}{2}n^2 - \frac{A\omega^3\cos(\varphi)}{6}n^3 + \ldots & (27) \end{aligned}$$

where n is a continuous variable. It is known that the Taylor expansion is the best polynomial expansion of the analyzed signal at $n = 0$. Let us now approximate the signal $y(n)$ with cubic polynomial

$$\hat{y}(n) = p_0 + p_1 n + p_2 n^2 + p_3 n^3 \tag{28}$$

where coefficients p_k are chosen in order to minimize the total approximation error over the whole considered time interval. Note, an unknown initial phase appears as $\sin(\varphi)$ in the even terms and as $\cos(\varphi)$ in the odd terms for the exponent n of a polynom $y(n)$.

If we divide the coefficient of n^2 by the constant term we obtain

$$\frac{-\frac{A\omega^2\sin(\varphi)}{2}}{A\sin(\varphi) + B} \tag{29}$$

and, for sinusoid offset $B = 0$, we get

$$\frac{-\frac{A\omega^2\sin(\varphi)}{2}}{A\sin(\varphi)} = \frac{-A\omega^2\sin(\varphi)}{2A\sin(\varphi)} = -\frac{\omega^2}{2}. \tag{30}$$

On the other hand, if we use coefficients of n and n^3 there is no need to have $B = 0$ since we have

$$\frac{-\frac{A\omega^3\cos(\varphi)}{6}}{A\omega\cos(\varphi)} = \frac{-A\omega^3\cos(\varphi)}{6A\omega\cos(\varphi)} = -\frac{\omega^2}{6}. \tag{31}$$

According to Equations 27 and 28, we can now estimate the frequency of the considered signal (for $B = 0$) as

$$\frac{p_2}{p_0} = -\frac{\omega^2}{2} \tag{32}$$

and we obtain

$$\omega_{estimated} = \hat{\omega}_1 = \sqrt{-\frac{2p_2}{p_0}}. \tag{33}$$

Similarly, but without the assumption of $B = 0$, we get

$$\frac{p_3}{p_1} = -\frac{\omega^2}{6} \tag{34}$$

and the estimation is

$$\omega_{estimated} = \hat{\omega}_2 = \sqrt{-\frac{6p_3}{p_1}}. \tag{35}$$

Let us now consider the case with $2N+1$ samples of the analyzed signal obtained for $-N \leq n \leq N$. The total approximation error is

$$e = \sum_{n=-N}^{N} |y(n) - \hat{y}(n)|^2, \tag{36}$$

where coefficients p_k are determined by minimizing e, i.e., by solving

$$\frac{\partial e}{\partial p_k} = 0 \tag{37}$$

for $k = 0, 1, 2, 3$.

Now the estimation error can be calculated as

$$\omega - \hat{\omega}_2 = \left(\frac{N^2 + N}{36} + \frac{1}{24}\right)\omega^3 + O(\omega^5) \tag{38}$$

Note that for small ω and $\omega N < 1$ the estimation error is small. For example, if we have $2N + 1 = 65$ samples of the sinusoidal oscillation with period $T = 256$, we get $\omega = \pi/128$. In this example we know the true frequency. When we approximate the data set with cubic polynom, we can find coefficients p_1 and p_3 and estimate $\hat{\omega}_2$. We can then calculate the estimation error $\omega - \hat{\omega}_2$. In this example, the estimation error is then $\omega - \hat{\omega}_2 = 0.00043$ with relative error of 1.8%. It should be noted in this example that the signal is 1/4 of the period of the analyzed sinusoid. We can even define a better estimator according to (38)

$$\hat{\omega}_3 = \hat{\omega}_2 + \left(\frac{N^2 + N}{36} + \frac{1}{24}\right)\hat{\omega}_2^3 \tag{39}$$

Here we replace the true frequency ω in the estimation error with the estimation $\hat{\omega}_2$.

3 Simulation

3.1 Example 1

Let us consider the discrete signal

$$y(n) = A\sin(\omega n + \varphi) \tag{40}$$

with simulation parameters $A = 0.9$, $\omega = 0.03$, $\varphi = 1.27$, $-32 \leq n \leq 32$. Let the signal be discretized over the interval $[-1, 1]$ with $M = 128$ discretization levels

$$y_D(n) = \frac{2}{M}\left[\frac{M}{2}y(n)\right] \tag{41}$$

where $[\cdot]$ denotes the nearest integer. Now choose $n = 0$ and perform the frequency estimation according to (5) for various values of lag k.

Figure 2 shows the analyzed signal and estimation results using Method-1. Figure 2a and Figure 2d illustrate an example with $M = 512$ discretization levels. Since the discretization noise estimation is inaccurate for small k, the highest possible lags k are used for the frequency estimation. The mean estimate over the range of lag $16 \leq k \leq 32$ is $\hat{\omega}_e = 0.0300$ with the relative error 0.01%. The estimation method-2 gives $\hat{\omega}_2 = 0.0291$ with the relative error 3.10%. After the correction according to (39), $\hat{\omega}_3 = 0.0298$ with the relative error 0.70%. A less than 5 percent error from the true value is considered to be an acceptable value for estimating m-D frequencies. More examples will be provided in this section.

The experiment is repeated with $M = 128$ discretization levels. Results are presented in Figure 2b and Figure 2e. The mean estimate over the range of lag (in time) $16 \leq k \leq 32$ is $\hat{\omega}_e = 0.0299$. The relative error of the mean estimate over the range of lag $16 \leq k \leq 32$ is 0.36%. The estimation method-2 gives $\hat{\omega}_2 = 0.0289$ with the relative error 3.70%. After the correction according to Equation (39), we get $\hat{\omega}_3 = 0.0296$ with the relative error 1.34%.

Figure 2c and Figure 2f illustrate the case with $M = 32$ discretization levels. The mean estimate over the range of time lag $16 \leq k \leq 32$ is $\hat{\omega}_e = 0.0295$. The relative error of the mean estimate over the range of time lag $16 \leq k \leq 32$ is 1.7%. The estimation method-2 gives $\hat{\omega}_2 = 0.0288$ with the relative error 4.09%. After correction according to (39), we obtain $\hat{\omega}_3 = 0.0295$ with the relative error 1.74%. These results show that when the number of discretization levels is high, both methods are in good agreement with the true value. When there is a limited number of discretization levels, the estimation method-1 provides reliable results at higher time lags while the estimation while method-2 provides consistent results. The estimation method-2 requires more data in order to perform accurate cubic polynomial approximation.

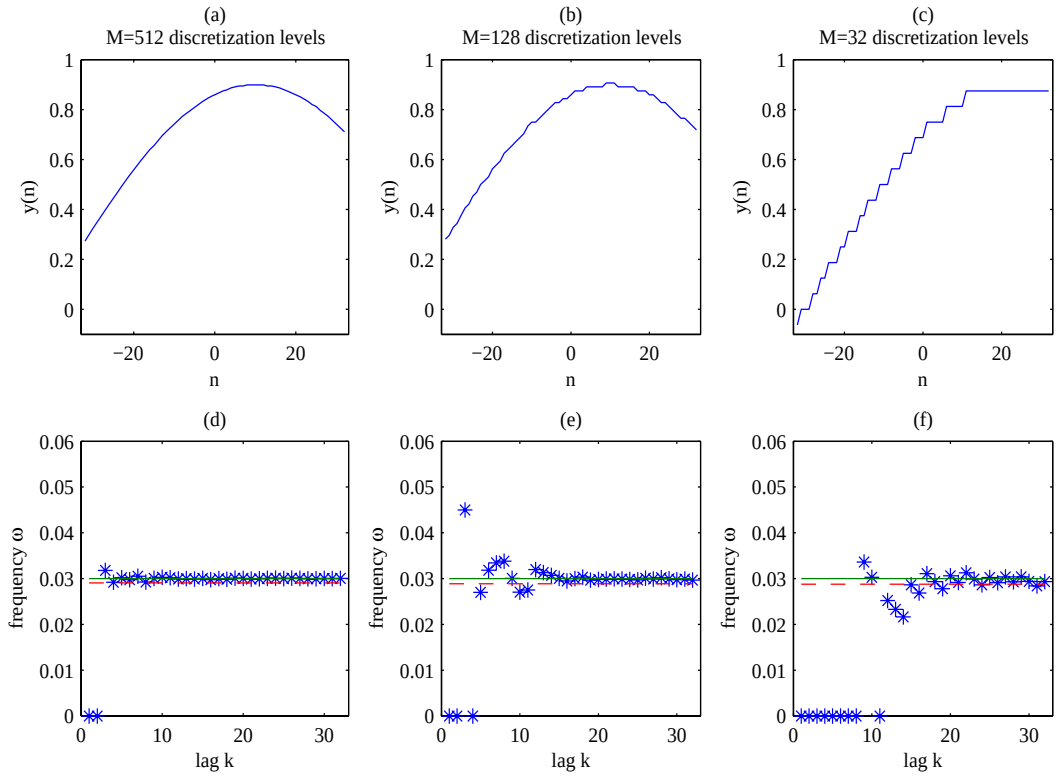

Figure 2: *Analyzed signal discretized with (a) 512 levels, (b) 128 levels, and (c) 32 levels. Estimation results for various lags k are obtained with (d) 512 levels, (e) 128 levels, and (f) 32 levels. The solid line represents the true value, asterisk represents the values estimated by method-1, and the dashed line represents the value estimated by method-2.*

3.2 Example 2

Let us now consider the sinusoidally frequency modulated signal of the form

$$x(t) = \exp(j64\sin(2\pi t - \frac{\pi}{3})) + \varepsilon(t) \tag{42}$$

over time interval $0 \leq t < 250\,\text{ms}$ sampled with $T = 1/512$. Assume the modulation frequency is 1 Hz. The discretized signal is of the form

$$x(n) = \exp(j64sin(\frac{2\pi}{512}n - \frac{\pi}{3})) + \varepsilon(n), \tag{43}$$

with $0 \leq n < 128$, where $\varepsilon(n)$ is the Gaussian white noise with variance σ_ε^2.

Figures 3a,b,c illustrate the results with $\sigma_\varepsilon^2 = 0$. We use the S-method in order to obtain the time-frequency representation of the analyzed signal (Figure 3a) [11]. The instantaneous frequency is estimated by using the maximum position of the time-frequency representation and is shown in Figure 3b. Here we can see the effect of discretization. The estimation of the modulation frequency is calculated using the estimation method-1 (Figure 3c). The mean estimate over the range of lag $40 \leq k \leq 63$ is $\hat{\omega}_e = 2\pi \cdot 0.99\,\text{Hz}$. The estimation method-2 gives $\hat{\omega}_2 = 2\pi \cdot 1.023\,\text{Hz}$. Figure 3d,e,f illustrate the results for $\sigma_\varepsilon^2 = 1$ i.e., for SNR=0 dB. The mean estimate over the range of lag $40 \leq k \leq 63$ is $\hat{\omega}_e = 2\pi \cdot 1.05\,\text{Hz}$. Using method-2, the estimated frequency is $\hat{\omega}_2 = 2\pi \cdot 1.09\,\text{Hz}$. These results show that at high SNR, the estimation method-2 provides reliable results and the estimation method-1 provides reliable results at higher time lags. At low SNR, the estimation method-1 provides better results at higher time lags while the estimation method-2 provides the results, where the accuracy is within 9 percent error from the true value. These results suggest that the estimation method-2 is sensitive to high noise level.

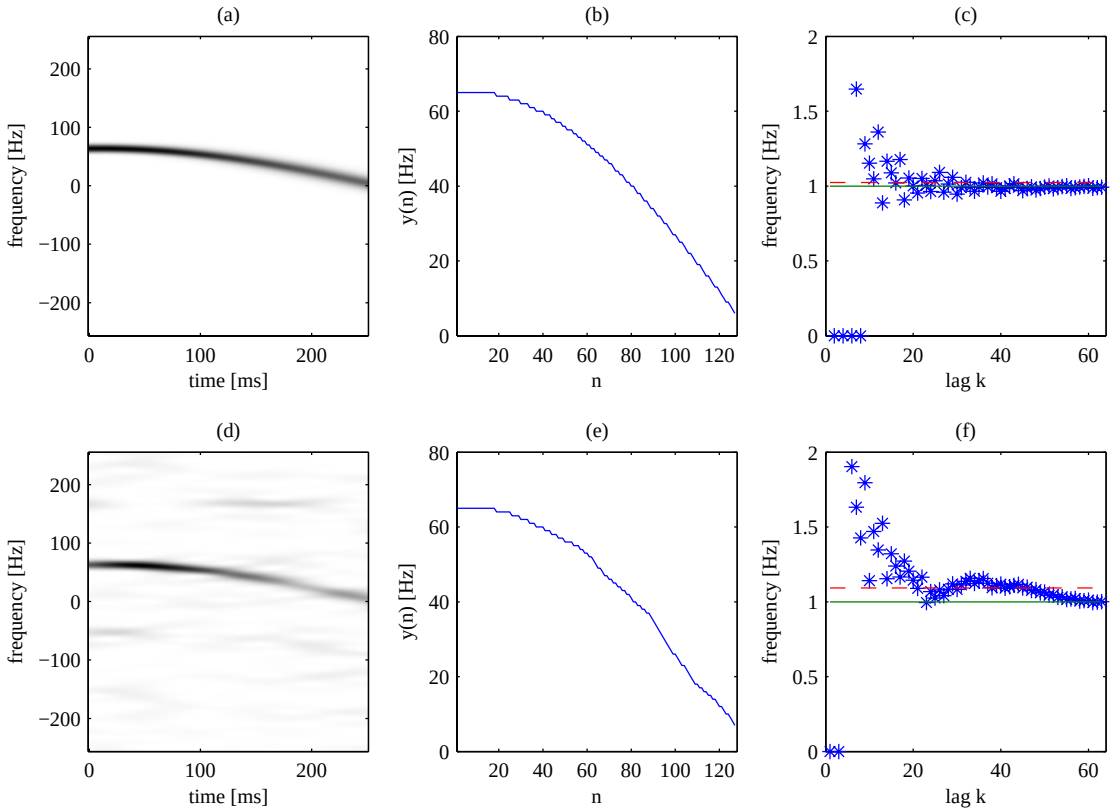

Figure 3: *Noiseless case: (a) time-frequency representation of the analyzed signal, (b) the instantaneous frequency of the signal, and (c) estimation results for various lags k. Noise case: (d) time-frequency representation of the analyzed signal, (e) the instantaneous frequency of the signal, and (f) estimation results for various lags k. The solid line represents the true value, asterisk represents the values estimated by method-1, and the dashed line represents the value estimated by method-2.*

3.3 UH-1D Helicopter

In this example we consider the simulated signal of a German Air Force Bell UH-1D Helicopter known also as 'Iroquois'. The simulation is performed according to [4]. Several effects are emphasized in the TF representation of Figure 4a. The stationary patterns along the time-axis correspond to the rigid body reflection, the vibration of the target or the radar-clutter caused by the movement in the target background. The motion of the two main blades is modeled by two rotating reflectors, producing sinusoidal FM signals with a large magnitude in the frequency direction. The main rotor flashes are simulated by the signals producing lines connecting peaks of the sinusoidal FM signal with time axis. The smaller pulses that can be seen in Figure 4a correspond to the tail rotor flashes. These flashes correspond to periodic alignment of the main and tail rotors to maximally reflect the radar signal. Note that other effects that can be observed in a radar image, including multipath, are not considered here.

Therefore, the simplified model of the reflected UH-1D signal can be written as:

$$x(t) = x_{RIG}(t) + x_{ROT}(t) + x_{FL\_M}(t) + x_{FL\_T}(t), \tag{44}$$

where $x_{RIG}(t)$, $x_{ROT}(t)$, $x_{FL\_M}(t)$ and $x_{FL\_T}(t)$ represent signals caused by the rigid body, rotation of the main rotor, and the main and tail rotor flashes, respectively. The signal is considered within the interval of 400 ms, sampled with a rate of $\Delta t = 1/48000$ s. Four sinusoidal components, caused by the rigid body, are at the frequencies -10.3 kHz, -2.5 kHz, 2.3 kHz and 2.7 kHz. Two components at -0.4 kHz and 0.4 kHz correspond to the modulated time tones commonly added to the data tape [12]. The sinusoidal FM signals, corresponding to the rotation of the main rotor blades, are modeled as:

$$x_{ROT}(t) = \sigma_{ROT}[\exp(j2\pi A_{ROT}\sin(2\pi t/T_{ROT})) + \exp(-j2\pi A_{ROT}\sin(2\pi t/T_{ROT}))]. \tag{45}$$

where $T_{ROT} = 175$ ms and $A_{ROT} = 19$ kHz. The main and tail rotor flashes are modeled as broadband pulses given as:

$$x_{FL\_M}(t) = \sigma_{FL\_M}\sum_k \delta(t - kT_{ROT}/2) *_\tau h_{FL\_M}(t) \tag{46}$$

$$x_{FL\_T}(t) = \sigma_{FL\_T}\sum_k \delta(t - kT_{TAIL}/2) *_\tau h_{FL\_T}(t), \tag{47}$$

where T_{TAIL} in our experiment is $T_{TAIL} = 35.8\,\text{ms}$, while $h_{FL\_M}(t)$ and $h_{FL\_T}(t)$ are cut-off filters given in the frequency domain as:

$$H_{FL\_M}(\omega) = \begin{cases} 1 & |\omega| < 2\pi A_{ROT} \\ 0 & \text{elsewhere,} \end{cases} \tag{48}$$

$$H_{FL\_T}(\omega) = \begin{cases} 1 & 2\pi(7.35\,\text{kHz}) < \omega < 2\pi(15.7\,\text{kHz}) \\ 0 & \text{elsewhere.} \end{cases} \tag{49}$$

The signal is corrupted with the moderate Gaussian noise. To compare our simulated radar image with the real one, refer to [4, 12].

In order to demonstrate our estimation methods, we have extracted a part of the helicopter data signal, which is presented in Figure 4b. The resulting instantaneous frequency estimation is shown in Figure 4c and the estimated frequency for various lag k is shown in Figure 4d. The mean estimated rotation per minute (rpm) over the range of lag $15 \leq k \leq 35$ is $\hat{\omega}_e = 352$. The estimation method-2 gives $\hat{\omega}_2 = 362$. The true value is 343 rpm. It should be noted that part of the discrepancy in the estimation value is caused by the noise and rigid body part (i.e., the horizontal line in the TF at approximately -5 kHz), which cause inaccurate IF estimation between n=53 and n=60 in Figure 4c.

We have repeated the procedure with different time instant n. In this case, two window sizes, narrow and wide windows, are used. The procedure is performed without additional noise and with additional noise. Results are presented in Figure 5 for noisy signals. Mean estimated rpm values using method-1 are 338 and 323 for the narrow and wide windows, respectively. Using method-2, mean estimated rpm values are 328 and 329 for the narrow and wide windows, respectively.

In Figure 6, results are presented for signals without additional noise. Mean estimated rpm values using method-1 are 349 and 348 for the narrow and wide windows, respectively. Using method-2, mean estimated rpm values are 329 and 330 for the narrow and wide windows, respectively. Both methods are in good agreement with the true value.

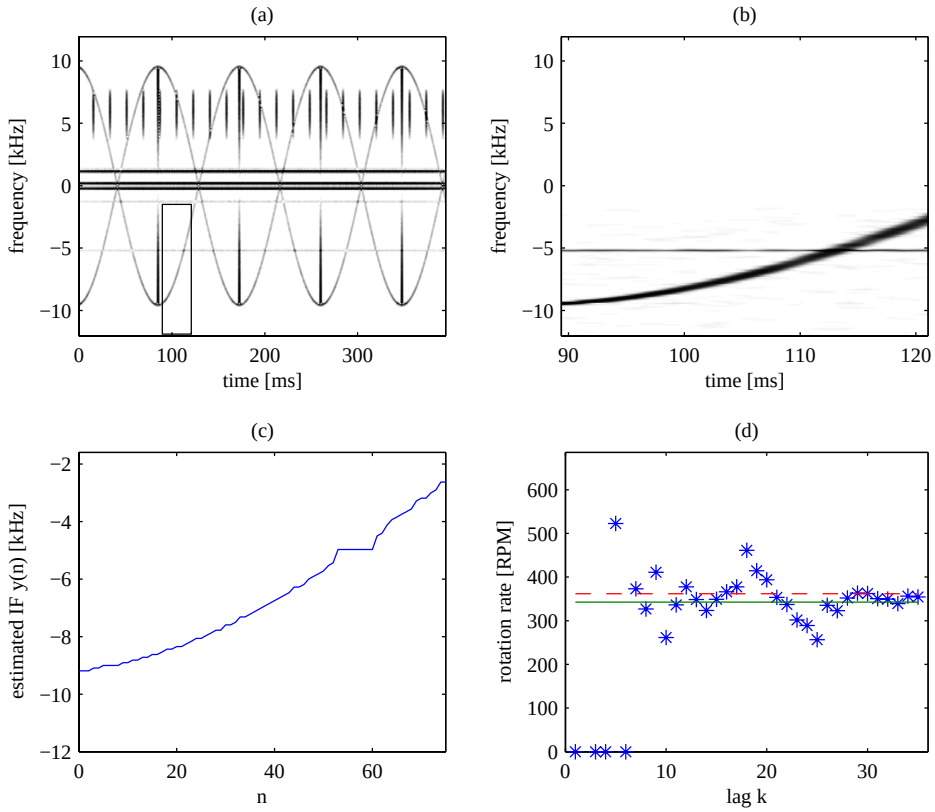

Figure 4: *(a) Time-frequency representation of the simulated helicopter data; (b) Part of the analyzed helicopter data; (c) The instantaneous frequency of the signal; (d) Estimation results for various lags k. The solid line represents the true value, asterisk represents the values estimated by method-1, and the dashed line represents the value estimated by method-2.*

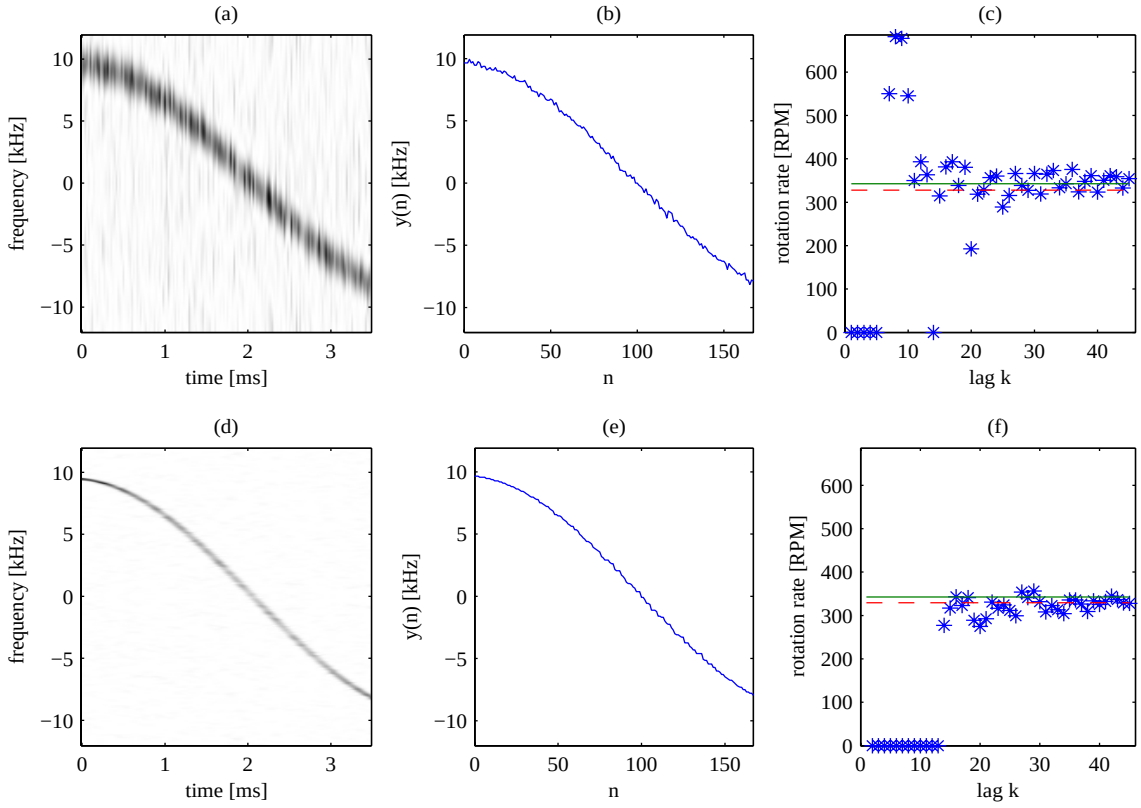

Figure 5: *Noise case using narrow window: (a) time-frequency representation of the analyzed signal, (b) the instantaneous frequency of the signal, and (c) Estimation results for various lags k. Noise case using wide window: (d) time-frequency representation of the analyzed signal, (e) the instantaneous frequency of the signal, and (f) estimation results for various lags k. The solid line represents the true value, asterisk represents the values estimated by method-1, and the dashed line represents the value estimated by method-2.*

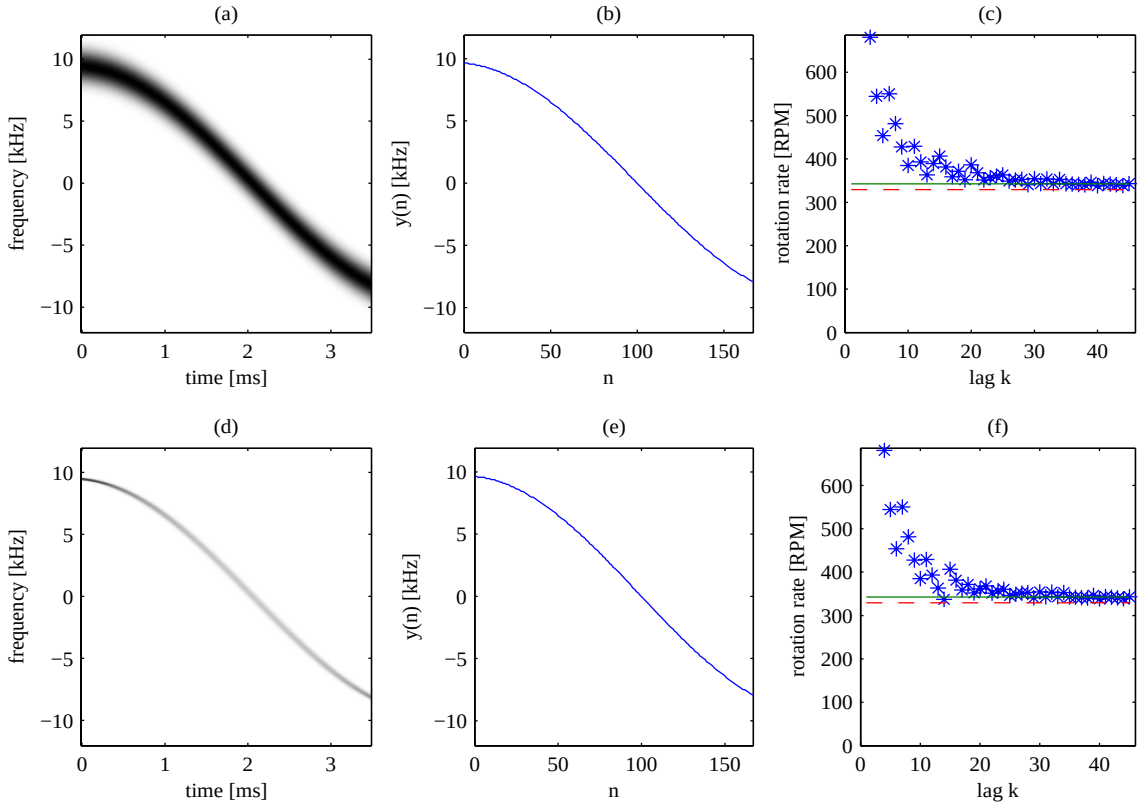

Figure 6: *Noiseless case using narrow window: (a) time-frequency representation of the analyzed signal, (b) the instantaneous frequency of the signal, and (c) estimation results for various lags k. Noiseless case using wide window: (d) time-frequency representation of the analyzed signal, (e) the instantaneous frequency of the signal, and (f) estimation results for various lags k. The solid line represents the true value, asterisk represents the values estimated by method-1, and the dashed line represents the value estimated by method-2.*

4 Experimental

4.1 Rotating fan

Experimental trials were conducted to investigate and determine the m-D radar signatures of objects that could be found in indoor radar imaging. The object in these experiments is rotating fan data supplied to us by Prof. Moeness Amin, Villanova University. The rotational motion of blades in a fan imparts a periodic modulation on radar returns. The rotation-induced Doppler shifts relative to the Doppler shift of the body occupy unique locations in the frequency domain. Whenever a blade has specular reflection such as at the advancing or receding point of rotation, the particular blade transmits a short flash or periodic modulation to the radar return. The rotation rate of the blade is directly related to the time interval between these flashes. The duration of a flash is determined by the radar wavelength and by the length and rotation rate of the blades. A flash resulting from a blade with a longer length and radar with a shorter wavelength will have a shorter duration.

The fan in this experiment is rotating at a height of approximately 2 m and at a range of 3 m from the radar. The fan has 4 metallic blades. The rotation rate of the blades is known to be 1050 rpm for this data. The experiment was conducted with the radar operating at frequency of 903 Hz. The sampling frequency is 5000 Hz.

Figure 7 illustrates the results. In order to demonstrate our estimation methods, we have extracted a part of the fan data signal, which is presented in Figure 7b. The mean estimated frequency over the range of lag $6 \leq k \leq 22$ is $\hat{\omega}_e = 7.55$ Hz. The estimation method-2 gives $\hat{\omega}_2 = 6.02$ Hz. After the correction, we get $\hat{\omega}_3 = 8.08$ Hz. The true value is 7.6 Hz.

4.2 Rotating corner reflector

Experimental trials were conducted to investigate and determine the m-D radar signatures of targets using an X-band radar. The target used for this experimental trial was a spinning blade with corner reflectors attached that were designed to reflect electromagnetic radiation with minimal loss. These controlled experiments can simulate the rotating types of objects, generally found in an indoor environment, for example, a rotating fan and outdoor environment, for example, a rotating antenna or rotors. Controlled experiments allow us to set the desired rotation rate and then permit us to cross check and assess the results.

The blade was set up to simulate real data that might be collected from a similar target such as a rotating antenna or rotating fan or any other rotation of structures on a target. The experiment was conducted with the radar operating at 9.2 GHz. The pulse repetition frequency (PRF) was 1 kHz. The target employed in this experiment

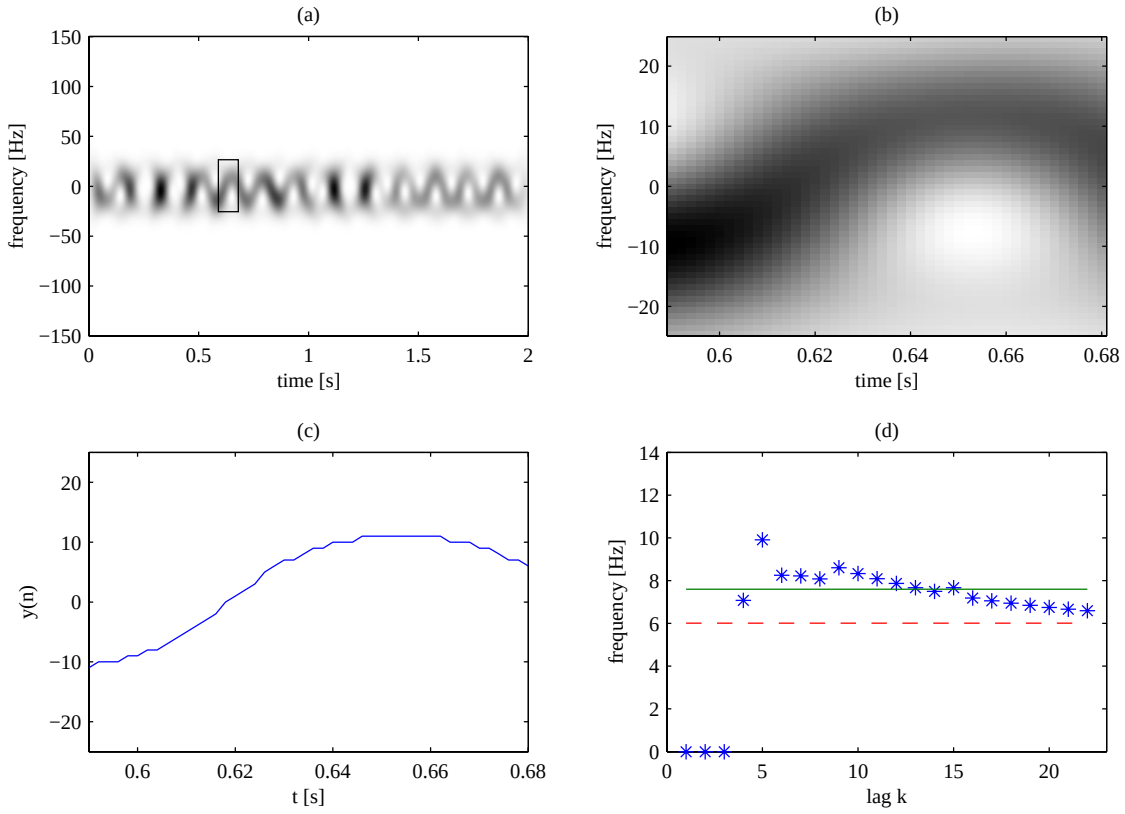

Figure 7: *(a) Time-frequency representation of the experimental fan data; (b) Part of the analyzed fan data; (c) The instantaneous frequency of the signal; (d) Estimation results for various lags k. The solid line represents the true value, asterisk represents the values estimated by method-1, and the dashed line represents the value estimated by method-2.*

was at a range of 300 m from the radar. The S-method is utilized in order to depict the m-D oscillation.

Figure 8 illustrates the results. In this case, the rpm of the corner reflector is 28. In order to demonstrate our estimation methods, we have extracted a part of the helicopter data signal, which is presented in Figure 8b. The mean estimated frequency over the range of lag $45 \leq k \leq 64$ is $\hat{\omega}_e = 26.19$ rpm. The estimation method-2 gives $\hat{\omega}_2 = 27.09$ rpm. After the correction, we get $\hat{\omega}_3 = 28.77$ rpm. In this case, method-2 shows excellent agreement with the true value while method-1 shows reliable results at higher time lags.

Figure 9 illustrates another example. In this case, the rpm of the corner reflector is 60. The mean estimated frequency over the range of lag $45 \leq k \leq 55$ is $\hat{\omega}_e = 60.65$ rpm. The estimation method-2 gives $\hat{\omega}_2 = 65.00$ Hz. After the correction, we get $\hat{\omega}_3 = 62$. In this case, method-1 shows excellent agreement with the true value.

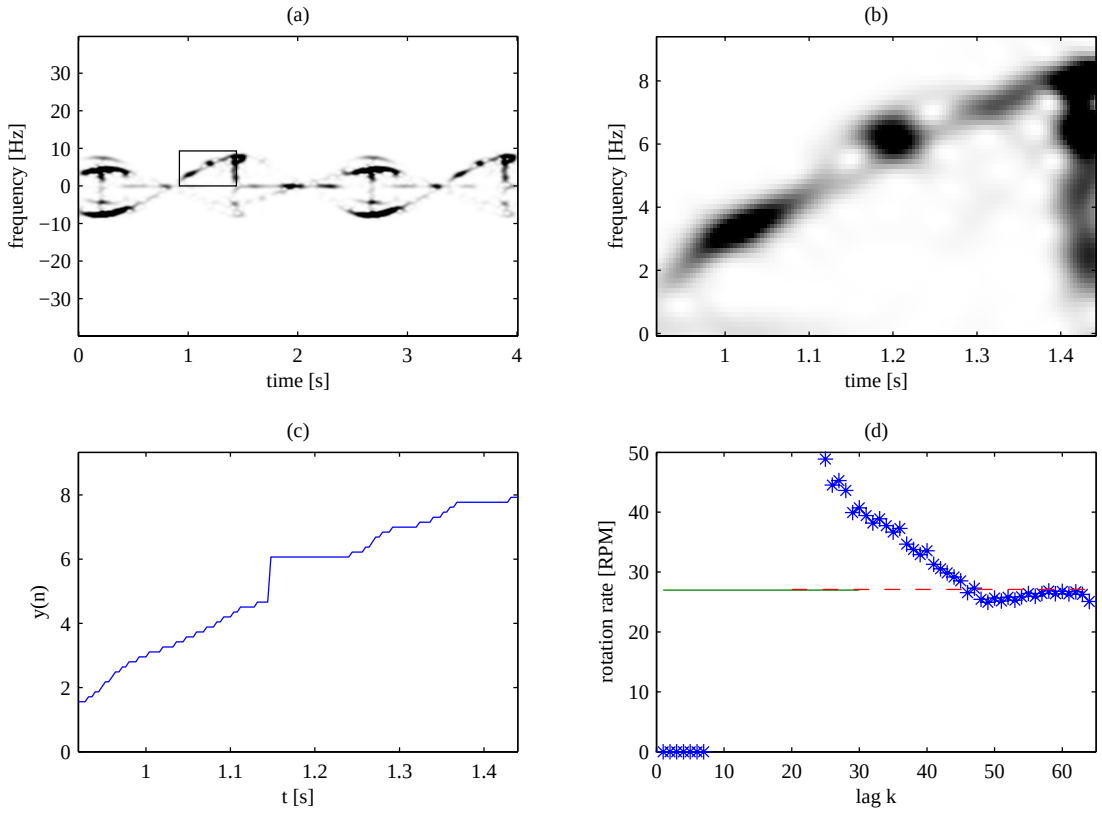

Figure 8: *(a) Time-frequency representation of the experimental corner reflector data; (b) Part of the analyzed corner reflector data; (c) The instantaneous frequency of the signal; (d) Estimation results for various lags k. The solid line represents the true value, asterisk represents the values estimated by method-1, and the dashed line represents the value estimated by method-2.*

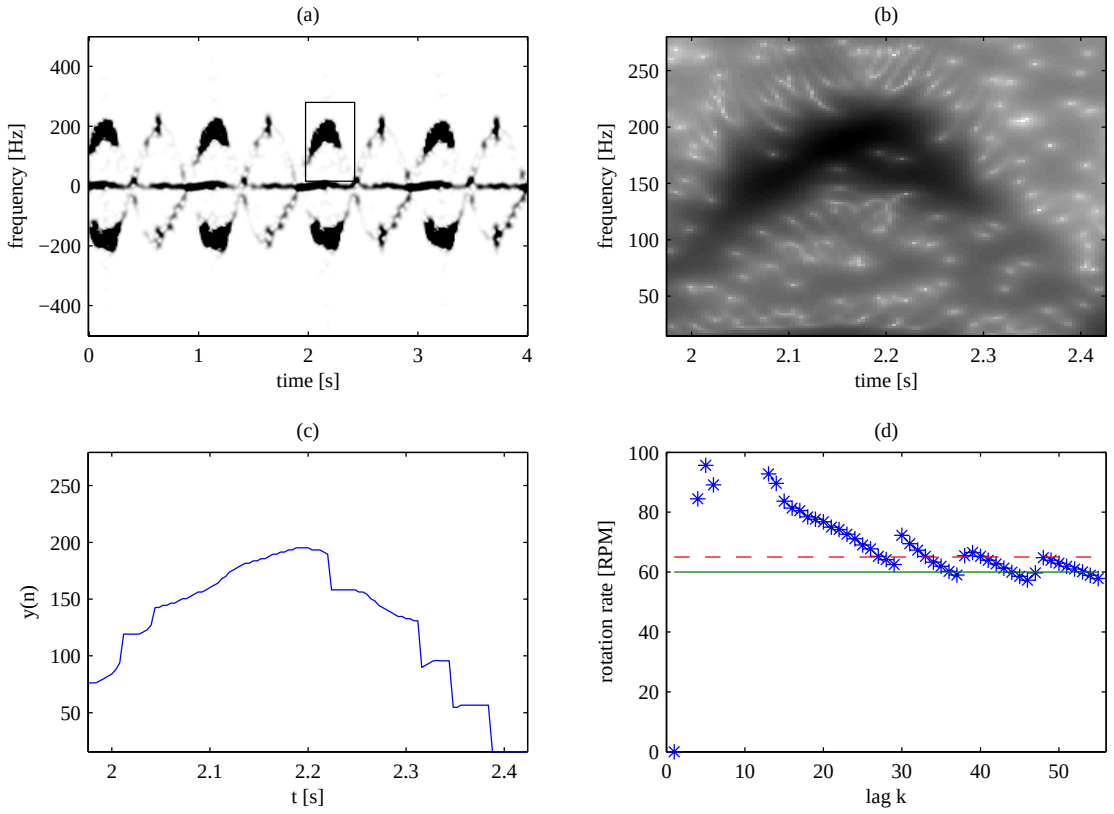

Figure 9: *(a) Time-frequency representation of the experimental corner reflector data; (b) Part of the analyzed corner reflector data; (c) The instantaneous frequency of the signal; (d) Estimation results for various lags k. The solid line represents the true value, asterisk represents the values estimated by method-1, and the dashed line represents the values estimated by method-2.*

5 Conclusion

The detection and extraction of micro-Doppler provide additional capability to better identify potential threats for security applications. Methods developed to extract micro-Doppler information for the past decade rely primarily on the assumption that the time series of the signal contains at least one oscillation or more during the coherent integration time or imaging time. However, real-world applications engage short duration signals and often require detection and estimation of micro-Doppler characteristics. Short duration signals may contain only a fraction of an oscillation. In this report, two methods for extracting micro-Doppler oscillation parameters have been proposed. In these scenarios, the coherent integration will cover only 1/4 and 1/2 of the oscillation. The first method is based on a three-point model and the second method is based on a cubic polynomial fitting and an approximation. The reliability and robustness of these two methods are evaluated using both simulated and experimental data. Both proposed methods have shown satisfactory accuracy for both simulated and experimental data.

Results from this study show that when the number of discretization levels is high, both methods provide reliable and robust estimation of the motion parameters. When there is limited number of discretization levels, the estimation method-1 provides reliable results at higher time lags while the estimation method-2 provides consistent results. The estimation method-2 requires more data in order to perform accurate cubic polynomial approximation. Both methods are sensitive to low SNR. Experimental results suggest that the estimation method-1 provides consistent reliable results at higher time lags compared to the estimation method-2, where the accuracy is within 5 percent error from the true value.

Micro-Doppler features have great potential for use in automatic target classification algorithms. Although there have been studies of m-D effects in radar in the past few years, this is the first study for micro-Doppler parameter estimation from a fraction of the period, that has great potential for use in target identification applications. As such, this report contributes additional experimental m-D data and analysis, which should help in developing a better picture of the m-D research and its applications to indoor and outdoor radar detection and automatic gait recognition systems. The two techniques developed in this study can be used to evaluate the motion parameters of the rotating antenna on a ship or ground using RADARSAT data. These techniques can also be used to extract biometric information related to periodic contraction of a heart, blood vessels, lungs, other fluctuations of the skin in the process of breathing and heart beating, which should help in human m-D research and its applications to through-wall radar imaging.

References

[1] V. C. Chen, and H. Ling, *Time-frequency transform for radar imaging and signal analysis*, *Artech House,* Boston, 2002.

[2] T. Thayaparan, S. Abrol, E. Riseborough, L. Stanković, D. Lamothe, and G. Duff. (2007), "Analysis of Radar Micro-Doppler Signatures From Experimental Helicopter and Human Data," *IEE Proceedings Radar Sonar Navig.,* 1, (4), pp. 288-299.

[3] T. Thayaparan, L. Stankovic., and I. Djurovic: "Micro-Doppler Based Target Detection and Feature Extraction in Indoor and Outdoor Environments, "*J. of the Franklin Institute,* 345, pp. 700-722, 2008.

[4] V. C. Chen, F. Li, S.-S. Ho, and H. Wechsler: "Analysis of micro-Doppler signatures," *IEE Proc. Radar, Sonar, Navig.*, Vol. 150, No. 4, Aug. 2003, pp. 271-276.

[5] V. C. Chen, F. Li, S.-S. Ho, and H. Wechsler, "Micro-Doppler effect in radar: phenomenon, model, and simulation study", Vol. 42, No. 1, pp. 2-21, *IEEE Trans. on Aerospace and Electronis Systems,*, 2006.

[6] T. Sparr, and B. Krane, "Micro-Doppler analysis of vibrating targets in SAR", *IEE Proc-Radar Sonar Navig.,* Vol. 150, No. 4, pp. 277-283, 2003.

[7] J. Li, and H. Ling: "Application of adaptive chirplet representation for ISAR feature extraction from targets with rotating parts", *IEE Proc. Radar, Sonar, Navig.*, Vol.150, No.4, August 2003, pp.284-291.

[8] T. Thayaparan, "Micro-Doppler analysis of the rotation antenna in airborne SAR image collected by the APY-6 radar," *IRS 2005*, Berlin, Germany, Sept. 2005.

[9] L. Stanković, T. Thayaparan, and I. Djurović, "Separation of target rigid body and micro-Doppler effects in ISAR imaging", *IEEE Trans. on AES,* Vol. 41, No. 4. pp. 1496-1506, 2006.

[10] P. Setlur, M. Amin, and T. Thayaparan: "Micro-Doppler signal estimation for vibrating and rotating targets," in *Proc. of ISSPA 2005*, Sydney, Austr. 2005, pp. 639-642.

[11] L. Stanković, "A method for time-frequency analysis," *IEEE Trans. Signal Process.*, Vol. 42, pp. 225-229, 1994.

[12] S. L. Marple: "Special time-frequency analysis of helicopter Doppler radar data", in *Time-Frequency Signal Analysis and Processing*, ed. B. Boashash, Elsevier 2004.

[13] B. Boashash, "Estimating and interpreting the instantaneous frequency of a signal - Part I," *Proc. IEEE*, Vol. 80, No.4, Apr. 1992, pp. 521-538.

[14] I. Djurović, and LJ. Stanković: "An algorithm for the Wigner distribution based instantaneous frequency estimation in a high noise environment", *Signal Processing*, Vol. 84, No. 3, Mar. 2004, pp. 631-643.

This page intentionally left blank.

DOCUMENT CONTROL DATA

(Security classification of title, body of abstract and indexing annotation must be entered when document is classified)

1. ORIGINATOR (The name and address of the organization preparing the document. Organizations for whom the document was prepared, e.g. Centre sponsoring a contractor's report, or tasking agency, are entered in section 8.)

Defence R&D Canada – Ottawa
3701 Carling Avenue, Ottawa ON K1A 0Z4, Canada

2. SECURITY CLASSIFICATION (Overall security classification of the document including special warning terms if applicable.)

UNCLASSIFIED

3. TITLE (The complete document title as indicated on the title page. Its classification should be indicated by the appropriate abbreviation (S, C or U) in parentheses after the title.)

Micro-Doppler signal estimation for rotating targets from a fraction of the period

4. AUTHORS (Last name, followed by initials – ranks, titles, etc. not to be used.)

Thayaparan, T.; L. Stankovic, M. D.

5. DATE OF PUBLICATION (Month and year of publication of document.)	6a. NO. OF PAGES (Total containing information. Include Annexes, Appendices, etc.)	6b. NO. OF REFS (Total cited in document.)
February 2010	40	14

7. DESCRIPTIVE NOTES (The category of the document, e.g. technical report, technical note or memorandum. If appropriate, enter the type of report, e.g. interim, progress, summary, annual or final. Give the inclusive dates when a specific reporting period is covered.)

Technical Memorandum

8. SPONSORING ACTIVITY (The name of the department project office or laboratory sponsoring the research and development – include address.)

Defence R&D Canada – Ottawa
3701 Carling Avenue, Ottawa ON K1A 0Z4, Canada

9a. PROJECT OR GRANT NO. (If appropriate, the applicable research and development project or grant number under which the document was written. Please specify whether project or grant.)	9b. CONTRACT NO. (If appropriate, the applicable number under which the document was written.)
12pz16	

10a. ORIGINATOR'S DOCUMENT NUMBER (The official document number by which the document is identified by the originating activity. This number must be unique to this document.)	10b. OTHER DOCUMENT NO(s). (Any other numbers which may be assigned this document either by the originator or by the sponsor.)
DRDC Ottawa TM 2009-280	

11. DOCUMENT AVAILABILITY (Any limitations on further dissemination of the document, other than those imposed by security classification.)

(X) Unlimited distribution
( ) Defence departments and defence contractors; further distribution only as approved
( ) Defence departments and Canadian defence contractors; further distribution only as approved
( ) Government departments and agencies; further distribution only as approved
( ) Defence departments; further distribution only as approved
( ) Other (please specify):

12. DOCUMENT ANNOUNCEMENT (Any limitation to the bibliographic announcement of this document. This will normally correspond to the Document Availability (11). However, where further distribution (beyond the audience specified in (11)) is possible, a wider announcement audience may be selected.)

Unlimited

13. ABSTRACT (A brief and factual summary of the document. It may also appear elsewhere in the body of the document itself. It is highly desirable that the abstract of classified documents be unclassified. Each paragraph of the abstract shall begin with an indication of the security classification of the information in the paragraph (unless the document itself is unclassified) represented as (S), (C), or (U). It is not necessary to include here abstracts in both official languages unless the text is bilingual.)

Radar micro-Doppler signatures are of great potential for identifying properties of unknown targets. All the techniques developed for extracting micro-Doppler features for the past decade rely primarily on the assumption that the time series of the signal contains at least one oscillation or more during the coherent integration time or imaging time. However, many applications in real-world scenarios involve short duration signals and often require the detection and the estimation of micro-Doppler characteristics. Short duration signals may contain only a fraction of an oscillation. In this report, we develop two techniques to estimate the micro-Doppler parameters from a fraction of the period. In these scenarios, the coherent integration will cover only 1/4 and 1/2 of the oscillation. The performance of the proposed methods are evaluated using both synthetic and experimental data.

14. KEYWORDS, DESCRIPTORS or IDENTIFIERS (Technically meaningful terms or short phrases that characterize a document and could be helpful in cataloguing the document. They should be selected so that no security classification is required. Identifiers, such as equipment model designation, trade name, military project code name, geographic location may also be included. If possible keywords should be selected from a published thesaurus. e.g. Thesaurus of Engineering and Scientific Terms (TEST) and that thesaurus identified. If it is not possible to select indexing terms which are Unclassified, the classification of each should be indicated as with the title.)

Micro-Doppler
S-method
Wigner Distribution
Short-Time Fourier Transform
X-band Radar
Three-point model
Cubic polynomial fitting

Defence R&D Canada

Canada's leader in Defence
and National Security
Science and Technology

R & D pour la défense Canada

Chef de file au Canada en matière
de science et de technologie pour
la défense et la sécurité nationale

www.drdc-rddc.gc.ca